

Terrestrial Laser Scanner imaging for the cyclostratigraphy and astronomical tuning of the Ypresian–Lutetian pelagic section of Smirra (Umbria–Marche Basin, Italy)



Marco Franceschi ^{a,*}, Luca Penasa ^a, Rodolfo Coccioni ^b, Jérôme Gattacceca ^c, Jan Smit ^d, Antonio Cascella ^e, Sandro Mariani ^f, Alessandro Montanari ^g

^a Department of Geosciences, Università degli Studi di Padova, Via Gradenigo, 6, 35131 Padova, Italy

^b Dipartimento di Scienze della Terra, della Vita e dell'Ambiente, Università degli Studi di Urbino 'Carlo Bo', Campus Scientifico 'E. Mattei', Località Crocicchia, 61029 Urbino, Italy

^c Jérôme Gattacceca, CEREGE, Avenue Philibert, BP 80, 13545 Aix-en-Provence Cedex 4, France

^d Vrije Universiteit, Faculty of Earth and Life Sciences, de Boelelaan 1085, 108HV Amsterdam, The Netherlands

^e Istituto Nazionale di Geofisica e Vulcanologia, Via della Faggiola 32, 56126 PISA

^f Gruppo Speleologico CAI Fabriano, Via Alfieri 9, 60044 Fabriano, Italy

^g Osservatorio Geologico di Coldigioco, 62021 Apiro (MC), Italy

ARTICLE INFO

Article history:

Received 2 February 2015

Received in revised form 20 August 2015

Accepted 21 August 2015

Available online 2 September 2015

Keywords:

Cyclostratigraphy

Terrestrial laser scanning

Biostratigraphy

Magnetostratigraphy

Ypresian–Lutetian

Astrochronological time scale

ABSTRACT

Terrestrial laser scanner imaging is applied, together with calcimetry and lithofacies logging, for the cyclostratigraphic characterization of the Ypresian–Lutetian pelagites exposed in the Smirra section (Umbria–Marche Basin, Italy). The necessary chronostratigraphic framework is provided by detailed bio- and magnetostratigraphic analyses, which allow locating the Ypresian–Lutetian boundary in this section. Terrestrial laser scanner intensity is compared to carbonate content values obtained through calcimetric analyses carried out on samples taken from the same section, and is found to represent a good proxy for lithology in these pelagic homogenites. Time-series analysis highlights Milankovitch frequencies, particularly evident in the high-resolution terrestrial laser scanner intensity series. The recognition of distinctive low-frequency (> 1 Myr) features in the amplitude oscillations of short eccentricity as well as its ~400 kyr modulation (long eccentricity), promote a tuning of the Smirra series using the most recent astronomic solution (La2010 nominal), which provides insights on the ages of the Y–L boundary and of the main biostratigraphic and magnetostratigraphic events in the Umbria–Marche Basin. Results confirm the value of high-resolution (mm-scale) terrestrial laser scanning for scrutinizing pelagite successions in search of low-frequency cycles that may help in the refinement of the astrochronological time scale.

© 2015 Elsevier B.V. All rights reserved.

1. Introduction

Cyclostratigraphy studies sedimentary cycles in the attempt to link them to periodic oscillations of Earth's orbital parameters, and relies on the widely accepted relationship between these oscillations, climate, and, consequently, sedimentation. This relationship has led to the successful recognition of orbital cycles in sediments (e.g. Herbert and Fischer, 1986) and has permitted the reconstruction of an astronomically calibrated time scale for the geological past (e.g., Hinnov, 2000; Hinnov and Ogg, 2007).

The reliability of cyclostratigraphic studies strongly depends on the length and resolution of the analyzed datasets (e.g. Hinnov, 2000, 2013). The longer and the more continuous a cyclic succession is, the better the cyclostratigraphy can be assessed. This poses a significant

challenge because the retrieval of long and high-resolution time-series can be time consuming and expensive. Moreover, it often occurs that the best sections are exposed on outcrops that are hardly or even not at all accessible for direct measurements (e.g. vertical cliffs, active quarry walls). To overcome this issue remote sensing approaches have been proposed. For instance, Schwarzacher (2005) used high-resolution photography, associating gray-scale values in photos to facies and producing gray-scale series for cyclostratigraphic analysis. More recently, Terrestrial Laser Scanner (TLS) imaging has emerged as a promising tool to rapidly obtain extremely high-resolution cyclostratigraphic data (i.e. proxy sampling at mm-scale), and proved particularly effective when dealing with long pelagic successions of limestone–marl alternations (Franceschi et al., 2011).

A Terrestrial Laser Scanner (TLS) produces a three dimensional representation of a target object in the form of a point-set, often referred to as a point cloud. The use of TLS intensity as a proxy for lithology was discussed in previous studies (e.g. Bellian et al., 2005; Franceschi et al., 2009, 2011; Burton et al., 2011). In particular, Franceschi et al. (2009)

* Corresponding author. Tel.: +39 3487691241.

E-mail addresses: marco.franceschi79@gmail.com, marco.franceschi@unipd.it (M. Franceschi).

showed that the intensity can be linked to the clay content in stratigraphic series composed of limestone–marl alternations and can be used to quantify lithologic variations along a stratigraphic section. The long range and high geometric accuracy of TLS make it particularly useful for cyclostratigraphy, because they allow a fast and precise imaging of sections even when exposed on vertical cliffs that may be not accessible otherwise. TLS acquisitions can be easily transformed into *intensity series* that are a convenient way to represent the variation of intensity and, hence, of the lithology, through a section. Then, these data are suitable for cyclostratigraphic spectral (FFT) analysis (Franceschi et al., 2011).

TLS provides a very accurate 3D representation of an outcrop. As consequence, the accuracy of stratigraphic thicknesses measured between intensity value in the intensity series is high and exceeds the one that is normally achieved with hand logging. This is an important feature with respect to cyclostratigraphy because a precise assessment of the sedimentary cycles in the space is the base for the correct interpretation of their temporal significance.

In this paper, TLS imaging is applied to the cyclostratigraphic analysis of the Eocene pelagic succession exposed in the Smirra section, in the Umbria–Marche Basin (northeastern Apennines of Italy). The section displays a continuous succession of well-bedded pelagic carbonates, which include layers of nodular radiolarian chert in its lower part. The chronostratigraphic placement of the section is obtained through magneto- and biostratigraphic (planktonic foraminifera and calcareous nannofossils) analyses that indicate the position of the Ypresian–Lutetian boundary according to its definition in the GSSP, which is established in the Spanish section of Gorrondatxe (Molina et al., 2011).

Results of calcimetric analyses (CaCO₃ wt.%) and lithologic logging carried out in the accessible portion of the section are compared with the intensity information provided by the TLS to evaluate similarities and differences of the cyclostratigraphic application of the three proxies. Time series on the basis of lithologic logging prove to have serious limitations when applied to homogenous calcareous sequences characterized by pseudo-bedding, and yield noisy cyclostratigraphic signals. Calcimetric analyses provide meaningful results, but could not be carried out on the entire section because of its exposure conditions. A strong positive correlation between chemical analyses and TLS shows that intensity values can be used as a proxy for lithologic variations. Compared to discrete calcimetric analyses, TLS allows higher resolution, better spatialization of the data, and coverage of the inaccessible parts of the outcrop.

The cyclostratigraphic analysis of the three proxies shows clear Milankovitch frequencies and is completed with astronomical tuning that anchors the Smirra section to the astrochronological time-scale, providing a cyclostratigraphic refinement of the timing of magnetic reversals and of some of the main biostratigraphic events in the Umbria Marche Basin.

Results of this study extend the effectiveness of the TLS approach to homogenous pelagic carbonate sequences widening the fan of possible applications of the technique beyond the contexts explored so far (Franceschi et al., 2009, 2011; Penasa et al., 2014). Embedding the TLS technique into an integrated stratigraphic analysis based on conventional methods enables a complete cyclostratigraphy across the Ypresian–Lutetian boundary in the Umbria Marche Basin. This provides useful insights for the refinement of the astrochronology of the period directly following the Early Eocene Climatic Optimum (EECO), the warmest period globally of the last 70 million years.

2. Geological setting

The section shown in Fig. 1A is exposed in a small abandoned quarry near the village of Smirra, about 4 km NE of the town of Cagli (coordinates: 43°35′09.40″N 12°40′37.30″E), in the Marche region of Italy (Fig. 1B). The exposed thickness of the Smirra section is about 26 m, where meter level 96.8 has been placed at the lowermost layer exposed on the quarry floor, meter 101 at the base of the vertical quarry front, and meter 123 at the highest layer exposed on the rim of the quarry (Fig. 1A). This is the best, most continuous and undisturbed exposure

known in the region of the stratigraphic interval comprising the contact between the R4 member of the Scaglia Rossa Formation and the overlying Scaglia Variegata Formation. The same stratigraphic interval is exposed in the Contessa Highway section near Gubbio (Lowrie et al., 1982), but exposition conditions make it not suitable for the application of TLS. In contrast to what was observed in the R2 member of the Scaglia Rossa (Galeotti et al., 2010), no evidence of hyperthermals (e.g. significant marly intervals) or other abrupt climate changes is found at Smirra. Conventionally, this lithostratigraphic contact is placed at the very last radiolarian chert horizon of the Umbria–Marche pelagic succession (Chan et al., 1985), which spans from the Triassic to the Late Miocene (e.g. Montanari et al., 1989, and references therein). This interval also comprises the chronostratigraphic boundary between the Ypresian and the Lutetian stages (i.e. the boundary between the Early and the Middle Eocene), which is here identified at meter level 109.6 on the basis of nannofossils and planktonic foraminiferal biostratigraphy coupled with magnetostratigraphy (see below, Fig. 2).

The lithologic transition from a calcareous Scaglia Rossa to a more marly Scaglia Variegata, apart from the presence–absence of chert, reflects the transition from a long lasting passive margin phase of the so-called Adriatic Promontory or Adria (D’Argenio, 1970), to the onset of the Alpine–Himalayan orogenesis in the Eocene. The Umbria–Marche basin was one of the epeiric marine basins formed on the subsiding Adria plate, originally located at a tropical latitude of 25°N in the Triassic, and subsequently migrating northward, reaching a latitude of 38°N in the Late Miocene (Dercourt et al., 1993, and references therein). The Umbria–Marche pelagic succession up to the Ypresian R4 member of the Scaglia Rossa, is mostly represented by biomicritic limestones which are made up of $\sim 93 \pm 5\%$ biogenic calcite (i.e. calcareous plankton), and an small siliciclastic component interpreted as wind-blown clay and silt particles (e.g. Arthur and Fischer, 1977; Johnsson and Reynolds, 1986). It is with the inception of the Alpine–Himalayan orogenesis that the Umbria–Marche basin started to receive terrigenous material, via runoff, from the surrounding uplifted continental areas of the southern European margin (i.e. the uplifting and emerging Alps; see Fig. 1C). Thus, the pelagic formations of the successions deposited during this orogenic phase show a general increase in the siliciclastic component, from an average of $\sim 20\text{--}30\%$ in the late Eocene Scaglia Variegata and the overlying Oligocene Scaglia Cinerea Formation, to $\sim 40\text{--}50\%$ in the mid Miocene Schlier Formation. This sedimentologic transition is also reflected by a change in bedding style. The carbonates of the pre-orogenic part of the Umbria–Marche succession, such as the Scaglia Rossa Formation, are to be considered pseudobedded homogenites, i.e. pelagic carbonate oozes homogenized by continuous syn-sedimentary bioturbation, which, during late diagenesis, assumed a layered structure, called pseudobedding, resulting from pressure-solution stylolitization along horizontal planes within the otherwise homogeneous carbonate sediment (Alvarez et al., 1985). On the other hand, the syn-orogenic formations such as the mid Eocene to Oligocene Scaglia Variegata and Scaglia Cinerea (e.g. Coccioni et al., 2008; Brown et al., 2009; Hyland et al., 2009), and the mid-upper Miocene Schlier Formation (e.g. Montanari et al., 1997; Cleaveland et al., 2002; Hüsing et al., 2010), have a rhythmite character, which is manifested by an alternation of distinct recessive marl and prominent limestone layers. In these formations, a marl–limestone couplet is interpreted to represent a precession cycle (e.g. Cleaveland et al., 2002; Hüsing et al., 2010). In the Smirra section the transition from a pseudobedded homogenite to a marl–limestone rhythmite occurs at meter level 120 (Fig. 1A).

3. Bio- and magneto-stratigraphy of the Smirra section

3.1. Biostratigraphy

3.1.1. Planktonic foraminifera

The analysis of planktonic foraminifera was carried out on a total of 27 samples spanning from meter level 97 to meter level 122.8.

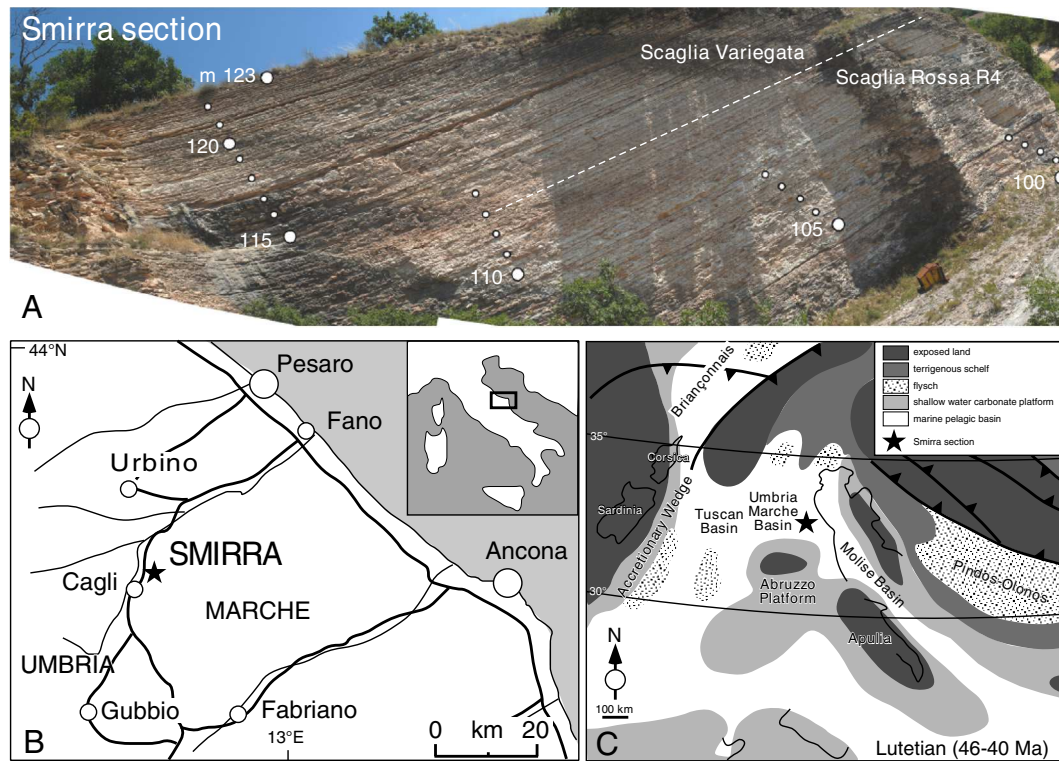


Fig. 1. A) The Smirra section exposing the transition between the Scaglia Rossa (R4 member) and the Scaglia Variiegata of the Umbria Marche Basin. White numbers are meter levels of the measured section (see Fig. 2); B) Location of the Smirra section (coordinates: 43°35′09.40″N 12°40′37.30″E); C) Paleogeographic map showing the position of the Umbria Marche Basin and of the surrounding paleogeographic domains in the Lutetian (Early Eocene).

Foraminifera from the > 63 μm size fraction were successfully extracted from indurated marly limestones and limestones using the cold-acetolyse technique of Lirer (2000) (Fig. 3), thus confirming its great potential for studies on indurated rocks, which otherwise, can only be analyzed in thin sections (e.g., Coccioni et al., 2004; 2006; 2007; 2012a,b; 2013; Jovane et al., 2007; Giusberti et al., 2009; Coccioni and Bancalà, 2012; Gardin et al., 2012). Planktonic foraminiferal assemblages are rich, diverse, and well preserved throughout the studied section. The taxonomic criteria here adopted mainly follow Pearson et al. (2006) and Payros et al. (2009), and the biostratigraphic zonal scheme of Wade et al. (2011) amended by Luciani and Giusberti (2014) is applied here.

The base of the Smirra section yields planktonic foraminiferal assemblages attributable to Zone E7a. The only planktonic foraminiferal zonal marker of the middle Eocene recognized in the Smirra section is *Turborotalia frontosa*. The lowest occurrence (LO) of this species marks the base of Subzone E7b and is a critical event for the Ypresian/Lutetian (Y/L) boundary placement, being estimated to be ~550 kyr older than the *Blackites inflatus* datum (Payros et al., 2009, 2010), which is the calcareous nannofossil horizon selected as the primary approximation marker in the Gorronatxe GSSP section where, unfortunately, a fault removes part of the boundary record (Molina et al., 2011).

The oldest specimens attributed to *T. frontosa* are quite rare and occur in our section at meter level 108.9, where we place the lowest rare occurrence (LRO) of this species. They have been classified here following the broad taxonomical concept of Payros et al. (2009) in which primitive specimens of *T. frontosa* show a slightly reduced size, a lower apertural arc, and a less inflated last chamber with respect to the typical morphotypes. At Smirra, the LRO of *T. frontosa* is recorded in the middle part of Chron C21r, thus in excellent agreement with the recent finding from the Possagno section in the Venetian southern Alps of northeastern Italy (Luciani and Giusberti, 2014). Above meter level 108.9, *T. frontosa* becomes more and more frequent with typical and common morphotypes occurring at 114 m (Fig. 3). At Smirra, the

lowest common occurrence (LCO) of this species lies at the top of Chron C21r, with a slight diachronism in respect to the Possagno section where evolute forms of *T. frontosa* are recorded by Luciani and Giusberti (2014) in the lowermost part of Chron C21n. Assemblages from the uppermost part of our section do not include common specimens of *Guembeltrioides nuttalli*, which marks the base of Zone E8 and therefore are still attributable to Zone 7b (Fig. 2).

3.1.2. Calcareous nannofossils

The analysis of calcareous nannofossils was carried out on the same collection of samples studied for planktonic foraminifera, prepared as standard smear slides (Bown, 1998). The taxa identification was done with a Leica DMLP 100 polarized-light microscope at 1250x magnification (Fig. 4). The abundance of each species was determined by counting 150–300 specimens and is expressed as percentage (see Table 1S in the Supplementary Material). Index species of *Discoaster* have been evaluated within 30–50 specimens of the genus. Moreover, at least two additional traverses, each 3 mm long, corresponding to 187 fields of view (FOV), were examined to recognize the presence of very rare index species. Microphotographs of significant taxa are shown in Fig. 4. The taxonomy of Perch-Nielsen (1985), Aubry (1999), and Bown (1998) was adopted, whereas the biozonations were those of Martini (1971, NP-Zones) and Okada and Bukry (1980, CP-Zones and Subzones).

Calcareous nannofossils at Smirra are generally rare, with an average of 2 specimens per FOV. Nannofossil specimens are moderately to poorly preserved with secondary overgrowth, and not all the specimens can be identified at the species level. Reworked Cretaceous and Paleocene species are generally very rare. The assemblages consist mostly of *Cyclargolithus floridanus*, *Sphenolithus* spp., and *Ericsonia formosa*. *Discoaster* spp. and *Coccolithus pelagicus* are also consistently present. *Coccolithus crassus*, *Psuedotriquetrorhabdulus inversus*, *Girgisia gammation*, *Dictyococites scrippse*, *Reticulofenestra* sp., *B. inflatus*, *Helicosphaera* spp. and *Toweius* spp. are rare to very rare. On the base

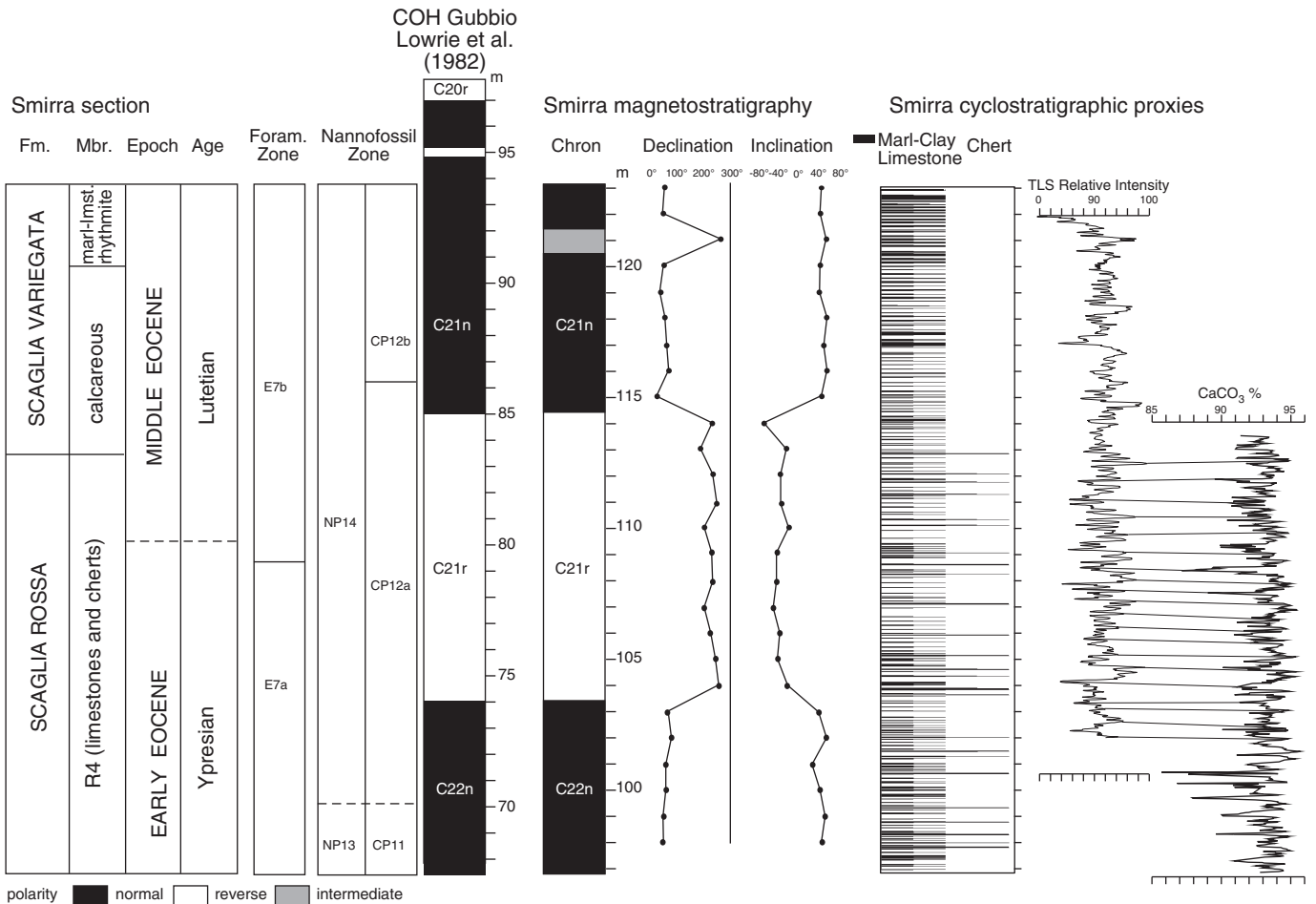


Fig. 2. Biomagnetostratigraphic scheme of the Smirra section correlated with the classic section of Gubbio, and the profiles of the three proxy series (lithologic series, CaCO₃ wt.%, and TLS intensity), which are used in this work for cyclostratigraphic analysis and astronomical tuning.

of the nannofossil assemblages, the Smirra section can be assigned to the SubZones CP12a and CP12b (Zone NP14), thus encompassing the Y/L boundary (Fig. 2; Table 1S). The LO of *B. inflatus*, which is considered a suitable marker for the approximation of the Y/L boundary (Larrasoña et al., 2008), and correlated with Chron C22r, is the only marker event detected here. Nevertheless, several additional events were recorded, which show a ranking comparable with that of the

Agost section (Spain), one of the candidate sections for the Lutetian Global Stratotype Section and Point (GSSP) (Tori and Monechi, 2013). Further detailed taxonomic and biostratigraphic information about the calcareous nannofossil genera identified in the Smirra section are contained in the online Supplementary Material.

3.2. Magnetostratigraphy

Oriented hand samples were obtained with a magnetic compass from 27 levels in the studied section (Fig. 2) with a sampling interval of one meter. They were drilled and cut in the laboratory to obtain two standard cylindrical paleomagnetic samples (25 mm diameter, 22 mm height) for each level. Natural remnant magnetization (NRM) was measured using a SQUID magnetometer (model 755R from 2G Enterprises) with a noise level of 10^{-11} Am². Samples were demagnetized using alternating field (AF) or thermal demagnetization, or a combination of both. Demagnetization data were evaluated using principal component analyses (Kirschvink, 1980). All paleomagnetic data were processed using PaleoMac software (Cogné, 2003).

The study of pilot samples showed that AF demagnetization was efficient in revealing the characteristic remnant magnetization (ChRM) after removal of a soft overprint up to 10 mT (Fig. 5). All remaining samples were demagnetized using AF. Eight samples out of 27 required a mild thermal demagnetization, up to 150 °C, to remove a magnetic overprint of probable viscous origin. Eventually, a well-defined ChRM could be defined for all sampled levels, and after tectonic-tilt correction we obtained 15 with normal polarity, 11 with reverse polarity, and one with transitional direction (Fig. 6). The polarity is normal from 97 to

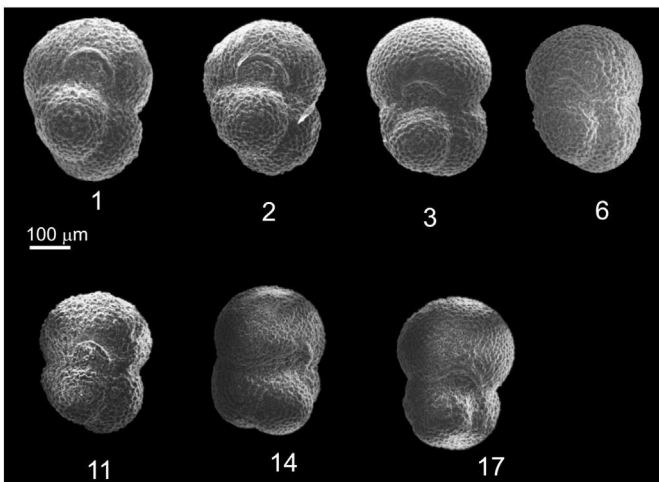


Fig. 3. *Turborotalia frontosa* from the Smirra section. A) Umbilical view, meter level 110; B) Umbilical view, meter level 120.

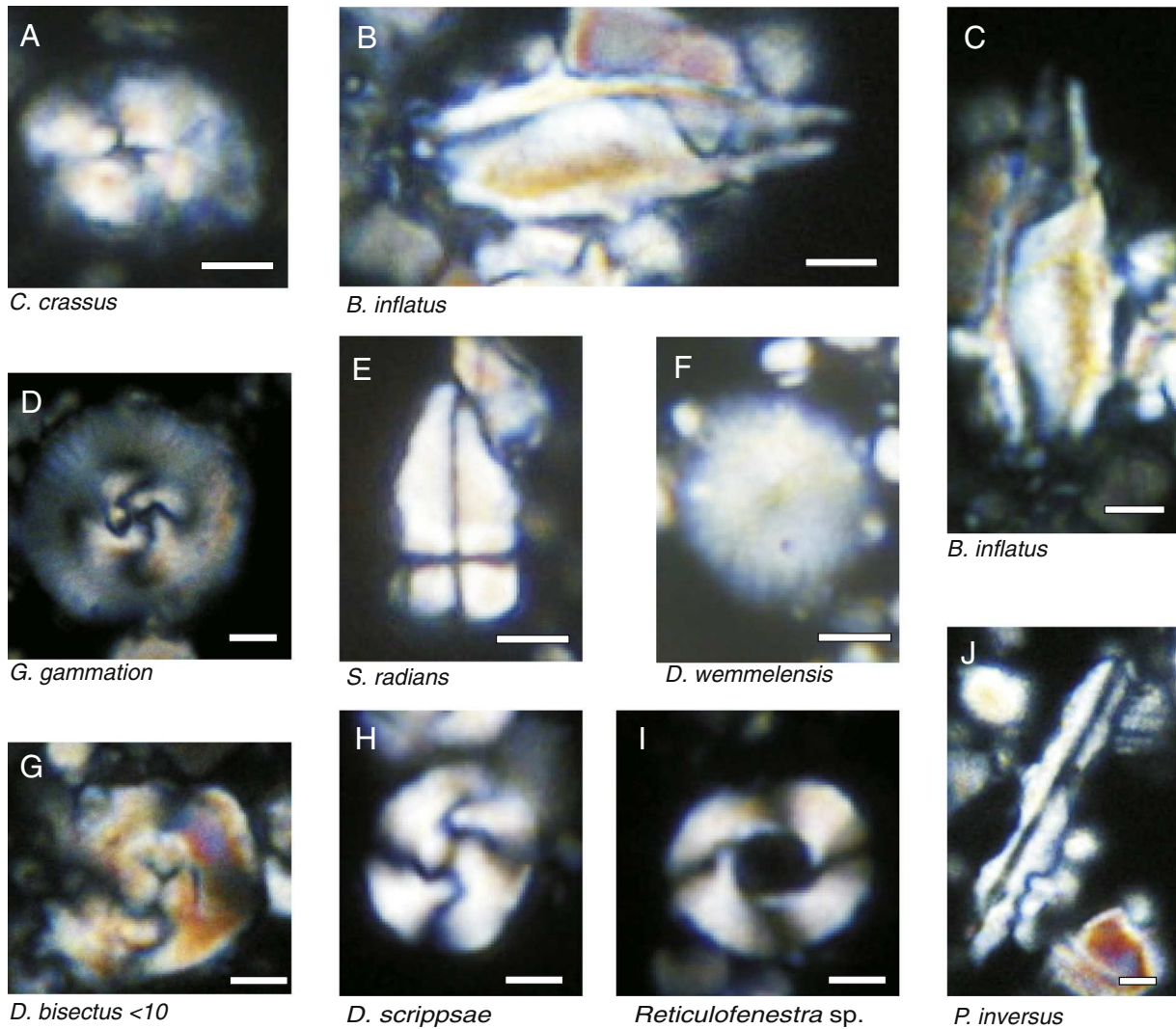


Fig. 4. Cross-polarized light microphotographs of selected calcareous nannofossils from the Smirra section. A) *Coccolithus crassus* Bramlette and Sullivan, 1961, meter level 98; B–C) *Blackites inflatus* (Bramlette and Sullivan, 1961) Kapellos and Schaub, 1973, meter level 116; D) *Girgisia gammation* (Bramlette and Sullivan 1961) Varol, 1989, meter level 111; E) *Sphenolithus radians* Deflandre in Grassé, 1952, meter level 112; F) *Discoaster wemmelensis* Achuthan and Stradner, 1969, meter level 108; G) *Dactyococites bisectus* (Hay, Mohler and Wade, 1966) Bukry and Percival, 1971, morphotype < 10 μm , meter level 112; H) *Discoaster scrippsae* Bukry and Percival, 1971, meter level 119; I) *Reticulofenestra* sp., meter level 118; J) *Pseudotrifarullus inversus* (Bukry and Bramlette, 1969) and Wise in Wise and Constans, 1976, meter level 118. Scale bar = 2 μm .

102.95 m, reverse from 104 to 114 m, and normal again from 115 to 123 m with the exception of the transitional direction at 121 m. The virtual geomagnetic pole (VGP) of this transitional direction makes a 97° (resp. 75°) angle with the mean of the normal- (resp. reverse-) polarity VGPs. The normal and reverse direction populations yield a positive reversal test (McFadden and McElhiny, 1990), strongly suggesting that the ChRM is a primary magnetization. The average normal paleomagnetic direction is $D = 54.8^\circ$, $I = 49.4^\circ$, $n = 15$, $A_{95} = 5.5^\circ$, $k = 49$ (n = number of samples, $_{95}$ = semi-angle of the 95% confidence cone around the mean, k = Fisher precision parameter). The average reverse direction is $D = 228.6^\circ$, $I = -40.0^\circ$, $n = 11$, $A_{95} = 14.4^\circ$, $k = 11.4$.

The overall paleomagnetic mean direction (in normal polarity) is $D = 52.0^\circ$, $I = 45.6^\circ$, $n = 21$, $A_{95} = 6.5^\circ$, $k = 19.9$. The paleomagnetic pole, computed as the mean of the VGPs from the 26 paleomagnetic directions, has longitude 105.0° , latitude 45.6° ($n = 26$, $k = 18.0$, $A_{95} = 6.9^\circ$). When compared to the African apparent polar wander path (Besse and Courtillot, 2002) this pole indicates a post-50 Ma counterclockwise rotation of $53.5 \pm 5^\circ$ with respect to Africa, whereas the shallowing is null ($0.8 \pm 3.2^\circ$) indicating no significant latitudinal movement with respect to Africa. This rotation is in broad agreement with the observed rotations in the study area (e.g., Muttoni et al.,

1998). The litho-biostratigraphic constraints of the Smirra section as compared to the reference Contessa Highway section at Gubbio of Lowrie et al. (1982) allows the confident identification of the lower normal polarity interval from levels 97 to 102.95 m as magnetochron C22n, the reverse interval from 104 to 114 m as C21r, and upper normal interval from 115 to 123 m as magnetochron C21n (see Fig. 2).

3.3. The Ypresian–Lutetian boundary at Smirra

The Ypresian–Lutetian chronostratigraphic boundary is established, with a golden spike, at meter level 167.85 in the GSSP of the Gorronatxe section, Spain (Molina et al., 2011), in correspondence to the lowest occurrence (LO) of *B. inflatus*, which defines the calcareous nannofossil biozonal boundary CP12a–CP12b of Okada and Bukry (1980). The golden spike is located within magnetochron C21r. C21r is only partially represented at the GSSP, because its base is at a fault contact at meter level 100, and the sediments at the footwall of the fault bear a normal magnetic polarity representing C22n (Molina et al., 2011). Unfortunately, *B. inflatus* seems to be absent or elusive in thoroughly studied pelagic sections in the Northern Apennines, such as the classic section of Contessa Highway at Gubbio (Lowrie et al.,

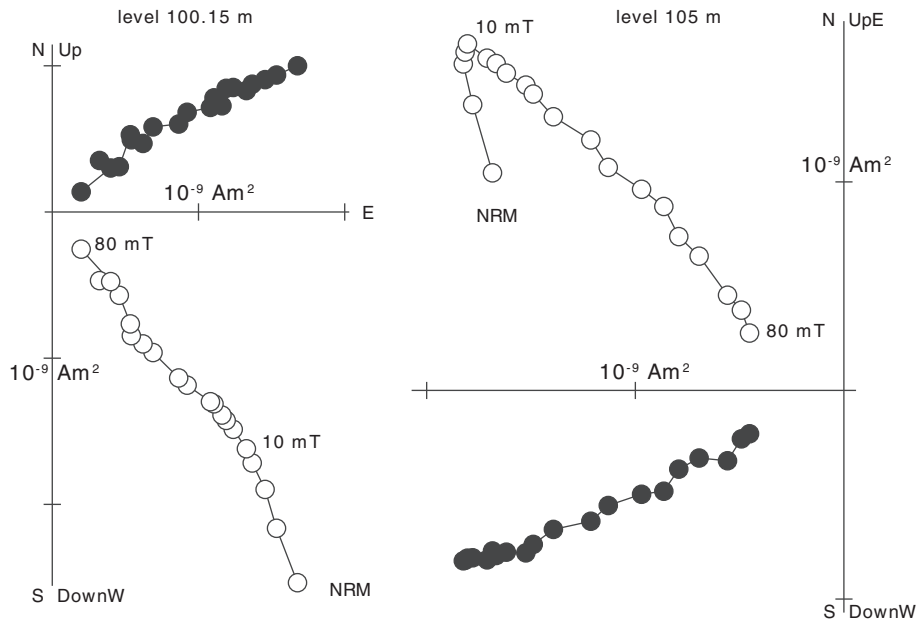


Fig. 5. Orthogonal projection plots of stepwise AF demagnetization data of representative normal- (level 100.15 m) and reverse- (level 105 m) polarity samples. Open and solid symbols represent projections on the horizontal and vertical plane respectively.

1982), or in the southern Alpine section of Possagno (e.g. Luciani and Giusberti, 2014, and references therein). Moreover, in the Smirra section, which is litho- and magnetostratigraphically identical to the nearby Gubbio section (in both C21r has the same thickness of 11 ± 0.5 m; see Fig. 2), the LO of *B. inflatus* is found well within C21n, and not somewhere in the middle of C21r where, in the GSSP of Gorrondatxe, it identifies the Ypresian–Lutetian boundary. In respect to the planktonic foraminiferal biostratigraphy, the GSSP's golden spike at Gorrondatxe is found within the *T. frontosa* Zone, the LO of which marks the E7a–E7b biozonal boundary of Wade et al. (2011). At Gorrondatxe the LO of *T. frontosa* is found in the lower part of C21r, at meter level 110, just 10 m above the fault; at Smirra the same datum is found in the middle of the complete C21r magnetozone at 108.9 m (see Fig. 2). Evidently,

biostratigraphic datums suggest a certain degree of diachronism among distant sedimentary successions from different marine basins, let alone different sedimentary facies (i.e. the Atlantic siliciclastic Flysch Formation of Gorrondatxe vs. the Tethyan pelagic limestone of the Scaglia Rossa Formation of Gubbio). The problem of precisely locating a chronostratigraphic boundary with respect to the integrated stratigraphy of an established GSSP can be solved using magnetostratigraphy, where magnetic polarity reversals can be considered synchronous worldwide within the analytical uncertainty of the method (i.e. sampling spacing, quality of the magnetic polarity signal).

In Fig. 7, we propose the placement of the Ypresian–Lutetian boundary at Smirra. The Gorrondatxe GSSP was correlated to the Contessa Highway section of Gubbio by normalizing the thickness of the complete C21n magnetic polarity zone, as represented by pelagic sediments in both sections. In order to do that, the 180 m thick C21n at Gorrondatxe was resized by eliminating ~13% turbiditic material using the sedimentological estimate of Payros et al. (2009) (e.g. see Fig. 3 in Molina et al., 2011). In the 62 m thick Lutetian portion of the C21r at Gorrondatxe, turbiditic material comprises a negligible ~2% of the bulk sediment, and resizing was not necessary. Such a correlation allowed a precise location of the Ypresian–Lutetian chronostratigraphic boundary at 109.6 m in the Smirra section, thus just 70 cm above the LO of *T. frontosa* (i.e. the E7a–E7b biozonal boundary of Wade et al., 2011).

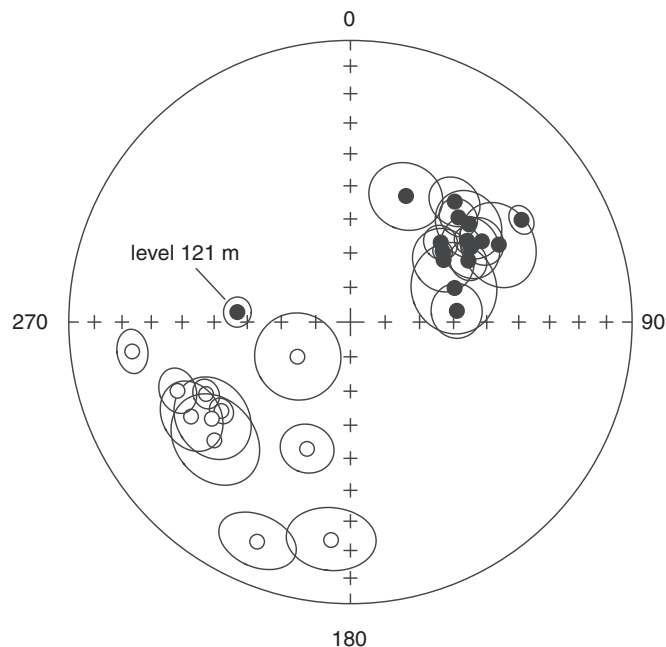


Fig. 6. Stereographic projection of the ChRM directions of the 26 studied levels. A transitional direction is indicated at meter level 121.

4. Cyclostratigraphic proxies at Smirra: TIs imaging, chemostratigraphy and lithologic logging

4.1. Lithologic logging

A detailed lithologic log of the Smirra section was constructed using a foldable carpenter meter stick to measure the thickness of limestones, chert layers and nodules, and recessive marl layers. Logging was carried out along the quarry exposure up to meter level 113 (Fig. 1). The rest of the section was measured by repelling with a rope down from the quarry's rim. Meter levels were marked on the outcrop with red spray paint and the outcrop photographed with a high resolution digital camera. The litholog was constructed considering three main lithologies: carbonate layers, marly layers, and chert. The resulting lithologic series is shown in Fig. 2.

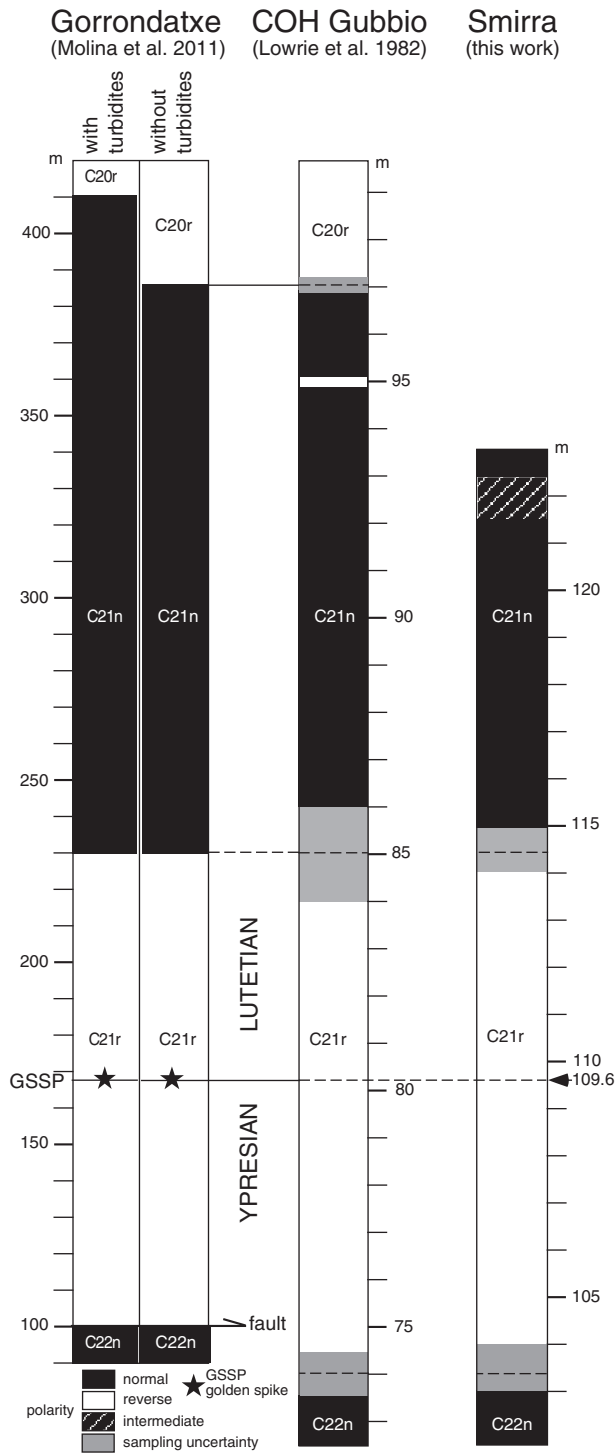


Fig. 7. Location of the Ypresian–Lutetian stage boundary in the Smirra section based on the biomagnostratigraphic correlation between this section, the GSSP of Gorrondatxe, and the classic section of Gubbio. See main text for further details.

4.2. Calcimetric analyses

Bulk rock samples (about 30 g each) were collected with hammer and chisel through the lower part of the section at an average spacing of 2.5 cm up to meter level 113 for a total of 668 samples. These samples were powdered with mortar and pestle and ~300 mg aliquots of <250 μm fraction were analyzed for total calcium carbonate content

(CaCO₃ wt.%) using a Dietrich-Furling water calcimeter with a precision of ± 2.5 wt.%. The resulting CaCO₃ wt.% curve is shown in Fig. 2.

4.3. TLS intensity series

Franceschi et al. (2011) showed that a convenient approach to the cyclostratigraphic study of Terrestrial Laser Scanner data is the construction of intensity series. An intensity series is a curve that represents the variation of the laser intensity along the considered stratigraphic section. In this study we used an Optech Illris 3D TLS (see Table 2S in the online Supplementary Material for detailed technical specifications). The Smirra section was scanned from a single station at a distance between 30 and 40 m, with an average density of 7000 points/m² on the target, with a sampling step on the surface of 12 mm (Fig. 8C).

The scan yielded a point-cloud with an average 5 mm point-to-point spacing (Fig. 8B). Before producing the intensity series (Fig. 8A), intensity values were corrected in function of the distance of the target from the acquisition position. Correction was obtained using the Kernel Smoothing approach (1.0 m bandwidth) suggested by Penasa et al. (2014). The backscattered intensity can be influenced by the angle of incidence of the laser beam with respect to the target, roughly correspondent to the angle between the target's surface and the TLS's line of sight. However, in this study we considered this effect as not relevant for two reasons. 1. Pesci and Teza (2008) regard this effect as negligible when dealing with targets characterized by natural roughness comparable to the laser's spot size. 2. Scans of the Smirra section were acquired in frontal position with respect to the outcrop, standing on an elevated ridge, further decreasing the effects of the incidence angle on the recorded intensity (Fig. 8C).

The intensity values refer only to the surface characteristics of the scanned rocks, thus they can be influenced and modified by several factors (e.g., surface weathering, dust, lichen or moss coatings, moisture). The point-cloud needs to be cleaned of undesired points before generating the final intensity series, and this was performed by removing all the irrelevant elements such as evident vegetation patches and areas covered by debris, following the procedure suggested by Franceschi et al. (2009, 2011).

Alteration and moisture on the outcrop result in visible intensity variations that are not related to lithological changes. When these surface alterations are present at a small scale (patches on the outcrop), their effect on the final time series is mitigated by averaging many points when the intensity series is generated (cfr. Franceschi et al., 2009, 2011). At Smirra, large-scale variations in intensity are visibly incoherent with the stratigraphy, which displays homogeneous lateral characteristics at the scale of the outcrop. Large-scale variations do not display lateral persistence, hence they are considered to be linked to alteration and/or moisture on the rock. In the intensity series the effect of these variations results in low frequency trends that are not related to variations in the lithology, which have to be removed before the time-series analysis. In the case of larger areas, their effect will produce low-frequency fluctuations in the final time series, which will result in a lower signal-to-noise ratio.

To cope with this problem a Gaussian smoothing low-pass filter ($\sigma = 1.0$ m) was applied to suppress undesired large-scale intensity variations. It is important to underline that the proposed procedure is tailored to the Smirra section. Other solutions could be evaluated case by case, on the basis of the characteristics of the specific outcrop. The removal of long-wavelength trends has to be carried out carefully to avoid the loss of true lithological variations. After the cleaning procedure, the final intensity-series was produced (Fig. 8A; Fig. 2).

To construct an intensity series, raw intensities were exported using the Optech Illris 3D proprietary parser as a 16 bit DN. The stratigraphic position of the points was defined by generating a plane in the space having the average strike and dip of the layering and calculating the orthogonal distance of each point from that plane. Hence, a running

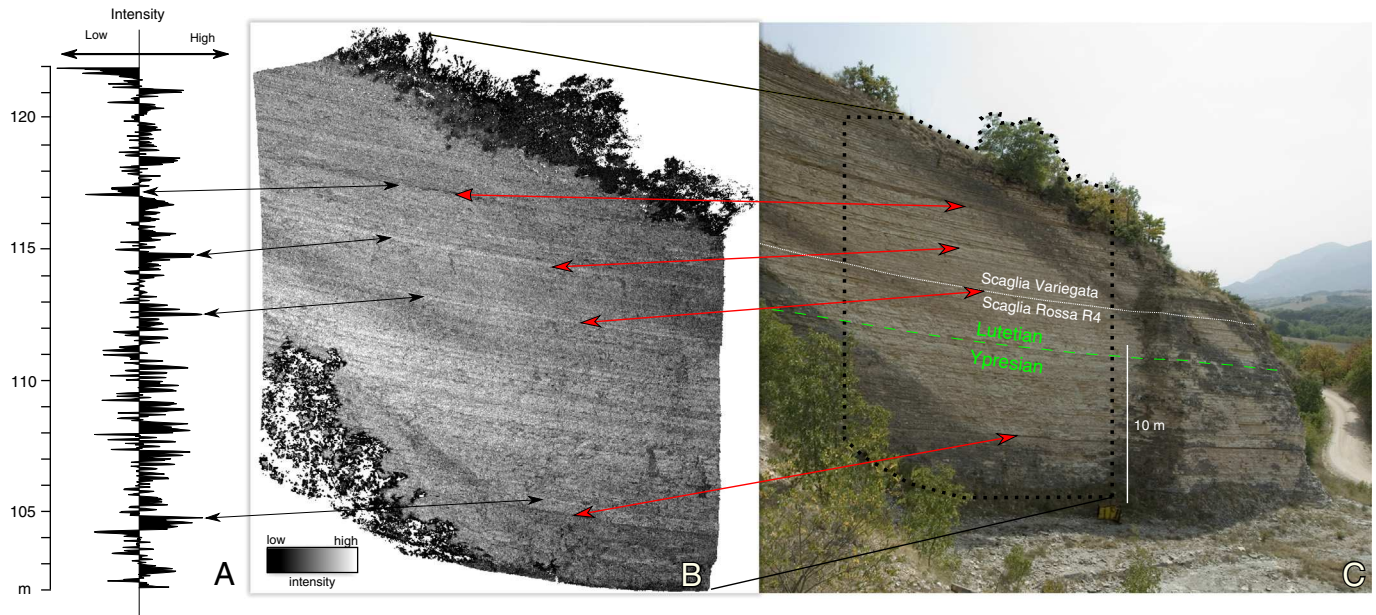


Fig. 8. A) Intensity series derived from the TLS acquisition of the Smirra outcrop. B) TLS point cloud of the Smirra quarry. C) Picture of the Smirra outcrop taken from the TLS scan station. The area scanned with the TLS is highlighted by the dark dotted line. The transition between the Scaglia Rossa (R4 member) and the Scaglia Variegata (white line) and the estimated position of the Y–L boundary (green dotted line) are also marked. Red and black arrows highlight corresponding layers the intensity series, point cloud and picture. (For interpretation of the references to color in this figure legend, the reader is referred to the web version of this article.)

weighted average was computed with the desired sampling step to generate a log (i.e. the intensity series) that represents the variation of intensities along the considered stratigraphic section. The intensity series was produced with a sampling step of 1.0 cm, employing the Kernel Smoothing method with a bandwidth of 1.0 cm (Fig. 8A). Each value of intensity derives from the averaging of the intensities of all the points of the point cloud located at a specific stratigraphic height in the section. As pointed out by Franceschi et al. (2011) this approach can be used effectively if the layering in the area considered for the intensity series generation displays uniform strike and dip. Where structural deformations such as folds or faults are present, they must be taken into account before the intensity series is generated with the method presented here. Another assumption is that the characteristics of each layer are homogeneous at the scale of the outcrop. This is necessary to obtain a log in which a certain stratigraphic height is associated with a representative intensity value. This can be considered a reasonable assumption for most pelagic carbonate series.

The final intensity series of the Smirra section is shown in Fig. 8A. In Fig. 2 intensity values are rescaled for comparison with the variations in CaCO_3 wt.%. The two curves shows evident correlation in their overlapping part, with maxima in TLS intensity corresponding to maxima in CaCO_3 wt.% and vice versa. This confirms the value of TLS intensity series as a proxy for lithology even when dealing with calcareous homogenites that do not display the clear lithologic alternations like limestone–marl couplets.

5. Cyclostratigraphy of the Smirra section

Spectral analysis was conducted on the TLS intensity, CaCO_3 wt.%, and lithologic series. Matlab™ algorithms modified from Muller and MacDonald (2000) were used to perform Fast Fourier Transforms (FFTs) in the space domain on detrended and zero-padded series (Bice et al., 2012). The statistical significance of spectral peaks was evaluated by generating a 95% confidence level from a Monte Carlo red noise simulation (Muller and MacDonald, 2000). This method was previously successfully applied for the cyclostratigraphic investigation of the Umbria–Marche basin succession in several studies (Cleaveland et al., 2002; Mader et al., 2004; Brown et al., 2009; Hyland et al., 2009). We

compared the results of the spectral analysis on the portion of the Smirra section covered by all the three proxies. Results are shown in Fig. 9A–C where highest spectral peaks of the Smirra proxies are labeled with their period expressed in centimeters. The persistence of the spectral peaks through the stratigraphic section was evaluated through evolutionary FFT spectra, performed on intervals of about one third of the entire stratigraphic series (Fig. 9D–F).

The power spectrum of the lithology log appears very noisy and shows spectral power scattered in several peaks at frequencies ranging from 4 to 12 cycles/m (Fig. 9A). The CaCO_3 wt.% series yields a less noisy spectrum, which is dominated by a prominent peak emerging well above the 95% confidence level with a period of 85.1 cm (Fig. 9B) This frequency peak is most powerful in the middle part of the section (see sliding window FFT in Fig. 9E). A less powerful signal with a period of 114 cm is present in the lower part of the section (Fig. 9E), whereas a relatively weak signal with a period wobbling around 240 cm is stationary through the lower 114 m of the Smirra section.

The power spectrum of the TLS intensity series is similarly dominated by a powerful frequency signal with a period of 85.1 cm (Fig. 9C), which appears to be stationary through this portion of the Smirra section, although it shows a relatively weak power in short stratigraphic intervals centered at 107.5 and 111 m (Fig. 9F). The TLS series displays also two prominent peaks (emerging above 95% c.l.) in the lower and upper parts of the analyzed section with periods of 184 and 245 cm. A relatively powerful peak is also revealed with a period of 17.3 cm between 106 and 107 m, but it appears to be rather unstationary throughout the rest of the section.

An average sedimentation rate of 9 ± 1 m/Myr for the Ypresian–Lutetian interval was estimated by Coccioni et al. (2012a,b) from the integrated biomagnetostratigraphy of the classic Contessa section at Gubbio, located a few tens of kilometers from Smirra. Hence, on the basis of this estimate, and assuming a mean sedimentation rate of 9 m/Myr for the coeval Smirra section, the dominant frequency peaks with a period of 85.1 cm emerging in both CaCO_3 wt.% and TLS intensity series would correspond to a time period of about 95.8 kyr, thus very close to the period of 95.1 kyr for the dominant short eccentricity frequency calculated in the La2004 astronomical solution by Laskar et al. (2004).

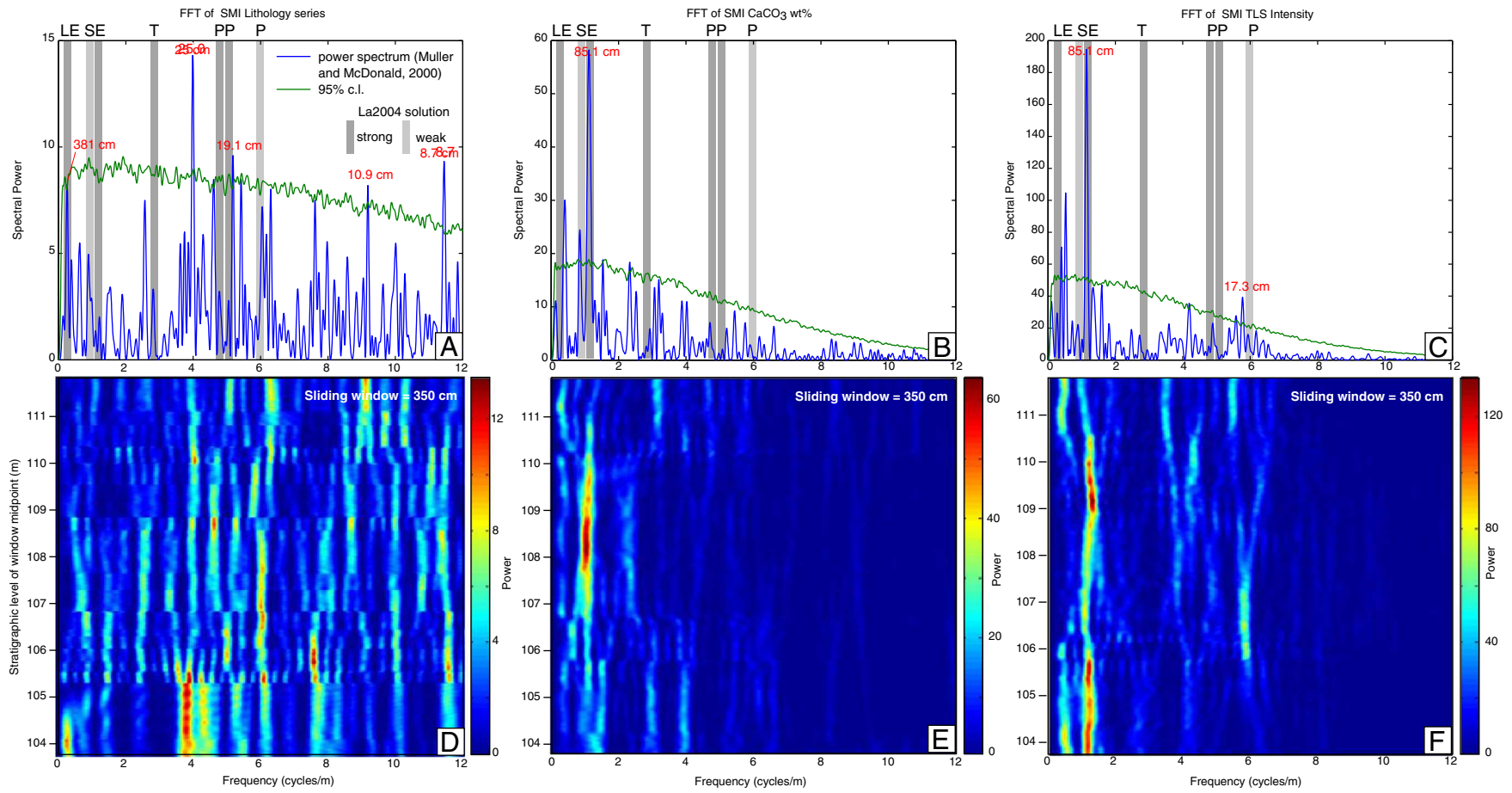


Fig. 9. FFT spectra of the cyclostratigraphy proxies considered at Smirra, for the interval in which they overlap. Algorithms from Muller and MacDonald (2000) were applied. A) Lithologic series; B) CaCO₃ wt.% series; C) TLS intensity series. Frequencies are expressed in cycles/m. Main spectral peaks exceeding the 95% confidence interval (green line) are labeled in red with their period expressed in centimeters. Gray vertical bands correspond to the expected spatial frequencies of the main Milankovitch cycles for the Eocene according to La2004 astronomical solution (Laskar et al., 2004) if an overall sedimentation rate of 9m/Myr is assumed. D); E); F) evolutionary spectra of the three proxies obtained by applying a sliding window FFT (window width = 350 cm). The presence of stationary spectral lines in the CaCO₃ wt.% series and in particular in the TLS intensity series corresponds to the 85.1 cycles/m frequency (SE).

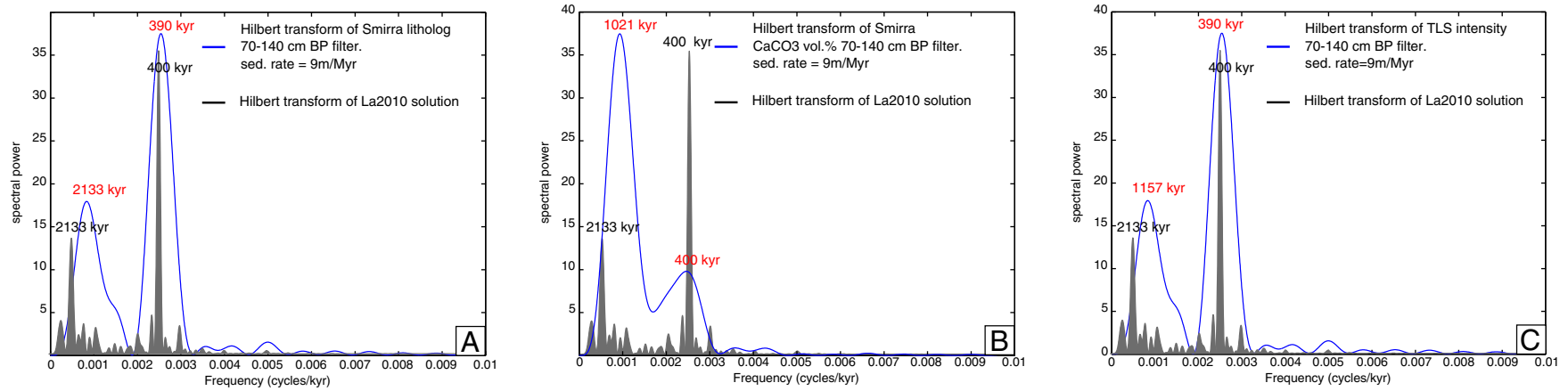


Fig. 10. Results of the Hilbert transform to highlight modulation of the frequencies in the SE (Short Eccentricity) band at Smirra (blue) and compare them to the SE modulation of [Laskar et al. \(2011\)](#) nominal astronomical solution (black). A) Lithologic series; B) CaCO₃ wt.%; C) TLS intensity series. In this case frequencies and periods are expressed in the time domain in cycles/kyr and kyr respectively. (For interpretation of the references to color in this figure legend, the reader is referred to the web version of this article.)

In order to have further confirmation of this cyclostratigraphic interpretation, we checked for modulations of the SE signal by the long eccentricity (LE) cycle. To do so, the Hilbert transform was applied on the three proxies series using a band-pass filter in the 70–140 cm frequency band. Results are shown in Fig. 10 A–C and display broad peaks that, with a mean sedimentation rate of 9 m/Myr, have periods of about 400 kyr. This corresponds to the expected LE amplitude modulation of SE and corroborates the cyclostratigraphic interpretation presented in this work.

6. Discussion

6.1. TLS vs other proxies

The application of a multi-proxy approach to the cyclostratigraphic study of the Smirra section allowed direct comparison of the results obtained by analyzing TLS intensity, CaCO₃ wt.%, and lithologic rank series (Fig. 9A–C). This reveals that TLS imaging provided better results in terms of accuracy in the stratigraphic positioning of the measurements, and in terms of spectral resolution. This is particularly evident when power spectra of the TLS data and lithologic rank series are compared (Fig. 9A and C). When calcareous homogenites are considered, the outcome of hand logging can be biased by the fact that pressure solution stylolites can be easily misinterpreted as true beds or thin marly interlayers. This bias is responsible for the very noisy spectrum of the lithologic rank series, with a spectral power concentrated at high frequencies, which is actually induced by the logging of the pseudobedding as marly interlayers.

The correlation of TLS intensity series with the CaCO₃ wt.% series is very good (Fig. 2). This implies that, in calcareous homogenites, TLS intensity can be used as a reliable proxy for detecting variations in the carbonate content relative to the siliciclastic terrigenous component. The TLS data cannot be used as they are, but they need to be pre-processed following the methodological procedure described above. It is worth noticing that sampling for CaCO₃ wt.% analysis was conducted in limestone layers only. Shales were not sampled, hence the curve (Fig. 2) represents variations in carbonate content within carbonate layers. This can be related to a cyclic increase and decrease in terrigenous content relative to primary biogenic carbonate (i.e. planktonic foraminifera and calcareous nannofossils). On the contrary, minima in the TLS series correspond to interlayers. The good correlation between the intensity series and the CaCO₃ wt.% curve, suggests that a decrease in calcium carbonate content within layers evolves to a shale interlayer.

The successful application of TLS to calcareous homogenites widens the possibilities of application of this technique, which was tested so far only in series with well developed limestone–marl alternations (Franceschi et al., 2011). Moreover, TLS allowed a complete cyclostratigraphic characterization of the section by analyzing the entire Smirra section whereas it was possible to carry out other investigations only in the limited accessible portion of the outcrop.

6.2. Astronomical tuning of the Smirra section

After having identified Milankovitch cycles in the Smirra section, it was possible to attempt to link it to the last available astronomical solution, La2010 nominal (Laskar et al., 2011).

The evolutionary FFT spectrum of La2010 nominal solution for the time interval between 45 and 52 Ma is shown in Fig. 11A. In the spectrum there occur time intervals in which SE displays clear modulations in power. A decrease in SE cycle power is accompanied by a contemporary rise in the power of LE. These *nodes* in SE do not seem directly related to the LE-induced (400 kyr) modulation and rather seem to reflect longer period (>1 Myr) amplitude modulation of the LE cycle. Several studies investigated these long-term modulations in the geologic record in an attempt to improve the link between sedimentary evidence of

cycles and eccentricity computations (e.g. Olsen and Kent, 1996; Lourens et al., 2005; Westerhold et al., 2007; Jovane et al., 2010). In the La2010 nominal solution the presence of one of the nodes (interval of low power) in the SE is predicted around 48 Ma, which is around the time encompassed by the Smirra section. Notably, a node characterized by a decrease in the LE power is also visible in the evolutionary spectrum of the Smirra TLS series (Fig. 11B) between meter levels 111 and 113. Given the magneto-biostratigraphic framework of the Smirra section that node could correspond to the one displayed by the La2010 nominal solution.

Confirmation that the node is a feature that reflects real lithological variation and not simply an artifact of the TLS intensity series is obtained by applying a band pass filter in the SE frequency to both the TLS and CaCO₃ wt.% series. The two filtered curves are shown in Fig. 12 and the node is clearly visible in both of them.

We used this feature of the power spectrum of the TLS series to tune the Smirra section to the La2010 nominal astronomical solution and pin it to the astrochronological time-scale of Gradstein et al. (2012). Further refinement of this correlation was obtained by considering the modulation induced in the SE cycle by the LE (~400 kyr). It was also necessary to determine the phase between the TLS intensity variation and the SE variation cycles displayed in the astronomical solution. TLS intensity and CaCO₃ wt.% series provide information on the relative variation of the terrigenous component at Smirra. High TLS intensity corresponds to high CaCO₃ content while, on the contrary, low TLS intensity corresponds to marly interlayers.

The cyclostratigraphic analysis carried out on the Maastrichtian pelagites of Zumaia by Batenburg et al. (2012 and references therein) suggests that the limestone/marl couplets are an expression of the precession cycle and are modulated by the SE. At Zumaia clays are interpreted as derived from continental runoff and show cyclic increase in their abundance that results in more or less developed couplets. This is interpreted to be caused by enhanced seasonality during eccentricity maxima that caused increased runoff. Peaks in the seasonal intensity resulted in more developed limestone/marl couplets and vice-versa. (Batenburg et al., 2012). It is generally accepted that the exiguous terrigenous component in the Scaglia pelagic limestone is aeolian in origin (e.g., Arthur and Fischer, 1977; Johnsson and Reynolds, 1986). This interpretation is consistent with the paleogeographic and geologic setting of the tropical U–M pelagic basin. This latter, from the early Cretaceous to the early Paleogene, was surrounded by large shallow water carbonate platforms (e.g. Dercourt et al., 1993), hence it seems unlikely that terrigenous input of fluvial origin would have been able to reach it. At Smirra, an increase of terrigenous fraction could similarly be related to an intensification of seasonal contrast that may have led to more intense trade winds during eccentricity maxima and a consequent increase of terrigenous wind-blown dust in the U–M pelagic basin. However, as shown in the palaeogeographic map in Fig. 1, orogenesis was ongoing to the NE and NW of the U–M basin. This certainly caused terrigenous input from continental runoff in the basins, hence a runoff-origin of the terrigenous at Smirra cannot be ruled out completely. In both cases however, whether the terrigenous component at Smirra was wind-blown or derived from runoff, enhanced seasonality during eccentricity maxima can be evoked as the driving process and led to the same inverse phase relationship between TLS and the eccentricity curves. Maxima of TLS intensity correspond to minima in eccentricity (low clay input) and minima of TLS intensity correspond to eccentricity maxima (high clay input). The results of the tuning based on the chosen phase relationship are displayed in Fig. 12. It might be argued that increased terrigenous input could have caused an increase in nutrients into the basins and, in turn, a rise in the carbonate production by coccolithophores. This may have acted in contrast to the enhanced input in of terrigenous fraction. Data presented in this study do not permit a detailed discussion of the climatic processes and of the interplay between terrigenous input and carbonate production. It should be noted, however, that the choice of a different phase relationship

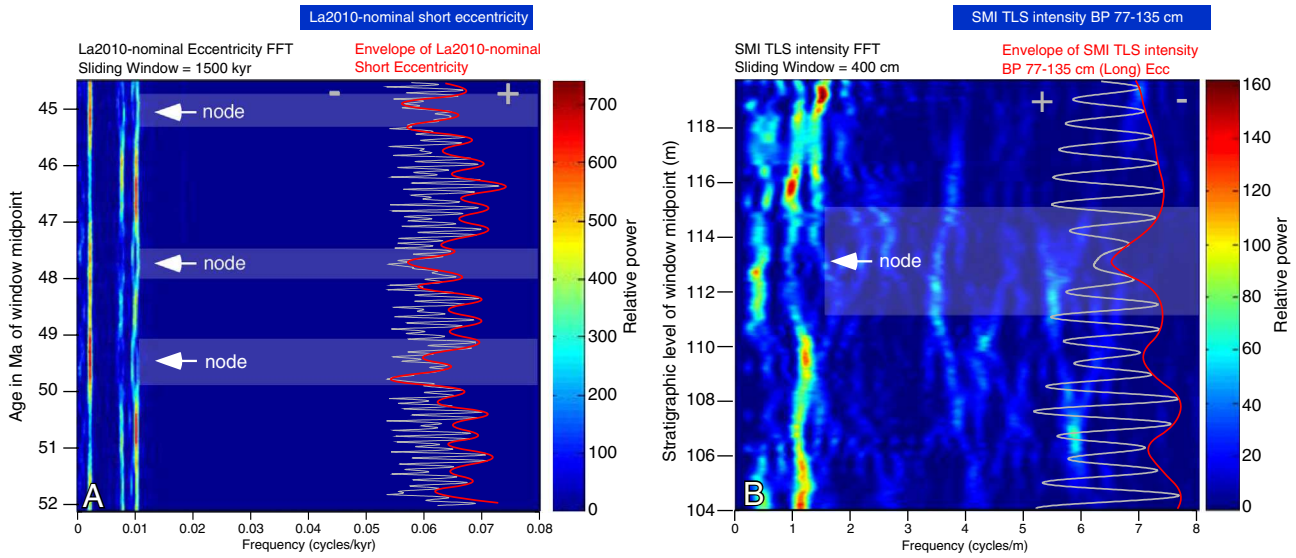


Fig. 11. A) Evolutionary spectrum of the La2010 nominal solution (Laskar et al., 2011) obtained applying a 1500 kyr-sliding window. The SE cycle (white line) is shown on the right along with its envelope (red line) to highlight SE amplitude modulations (~400 kyr). The position of evident nodes (intervals of low power in the SE) are marked by white arrows; B) Evolutionary spectrum of the Smirra TLS intensity series (sliding window 400 cm). On the right the result of band pass filtering of the frequency interpreted as the SE (white line) and the envelope highlighting its amplitude modulations (~400 kyr) (red line) are shown. The node in the power of the SE (white arrow) corresponds to the node visible in La2010 nominal astronomical solution. (For interpretation of the references to color in this figure legend, the reader is referred to the web version of this article.)

between TLS and SE would result in a difference in the tuning of only 50 kyr, i.e. half a SE cycle.

The astrochronological tuning shown in Fig. 12 highlights a slight discrepancy between the age of the Y–L boundary in the GTS-2012

(Gradstein et al., 2012). In GTS-2012 the current age of the Y–L boundary is set at 47.8 ± 0.2 Ma on the basis of extrapolated radioisotopic dates (Gradstein et al., 2012, and references therein). The position of the Y–L boundary at Smirra, obtained through integrated

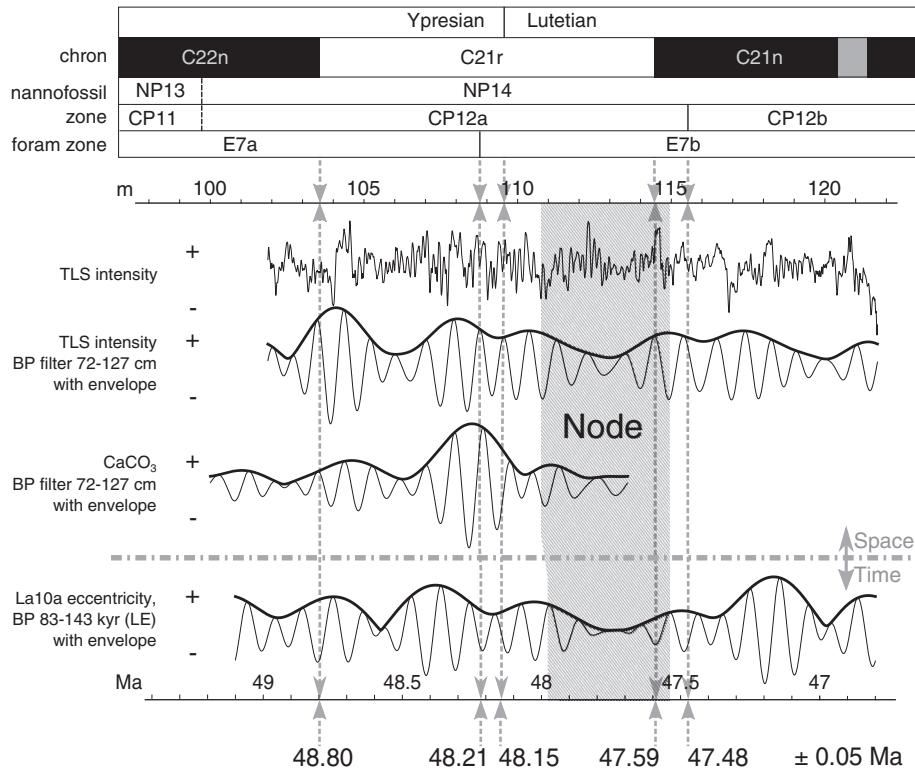


Fig. 12. Proposed tuning of the Smirra section on the La2010 nominal solution (Laskar et al., 2011). The tuning is based on the proposed phase relationships between the insolation curve and the TLS intensity curve (see main text for details). Band pass filters of SE frequency in the TLS and CaCO₃ wt.% (72–127 cm) are shown to highlight that the node displaying a decrease in the amplitude of the SE cycle is visible in both curves. The two key-elements for the tuning are the LE modulation of the SE cycle at Smirra and the node identified in the TLS series, correlated to the low frequency modulation of the SE displayed by the La2010 astronomical solution (see Fig. 11). According to the proposed tuning, the ages of the Y–L boundary, of the main biostratigraphic events and of the magnetic reversals identified at Smirra are labeled.

biomagnetostratigraphy (Fig. 7), and the cyclostratigraphic tuning on the La2010 nominal astronomical solution suggest for it an age of 48.15 ± 0.05 Ma. On this basis, numerical ages for other bio- and magnetostratigraphic events across the Ypresian–Lutetian boundary are proposed in Tab. 1. We present these results with the caveat that the relatively short stratigraphic interval encompassed by the Smirra section allows for the identification of only one node of the low frequency SE modulation. Nevertheless, the results in the cyclostratigraphic analysis obtained through the application of TLS imaging indicate that this technique could be a valuable tool to investigate long stratigraphic series, which are required to characterize low frequency modulations of Milankovitch cycles that may help in refining the astrochronological time scale.

7. Conclusions

Cyclostratigraphic analysis of the Smirra section was carried out using three independent proxy series, TLS intensity, calcimetry, and lithologic series. Comparison of the three techniques points out that TLS provides the best results, with better data positioning in the space and higher resolution. TLS intensity is confirmed as a valuable proxy for lithology even in stratigraphic series composed of calcareous homogenites that can pose significant challenges when studied by traditional hand-logging.

Biostratigraphy and magnetostratigraphy allowed the determination of main nannoplankton and foraminifera distributions, and the identification of main magnetic reversals in the section. This permitted to propose a positioning of the Ypresian–Lutetian boundary in the Smirra section.

The cyclostratigraphic interpretation shows the presence of strong cyclicities that are compatible with the expected Milankovitch frequencies for the Eocene (Fig. 9). In particular, SE was found to be the main cycle reflected in the stratigraphy, and displayed the expected LE amplitude modulation (Fig. 10).

Furthermore, spectral analyses of the TLS series highlighted features that are compatible with low frequency modulations of the main Milankovitch cycles (Figs. 11 and 12). Despite the limited length of the stratigraphic interval encompassed by the outcrop, it allowed to anchor the Smirra section, and hence the identified Ypresian–Lutetian boundary, to the latest astronomical solution for the Eocene. This permitted to propose refined ages of the main biostratigraphic events and magnetic reversals in the Umbria–Marche Basin (Table 1).

These results suggest that the integration of classical techniques with TLS imaging may help in the interpretation of the cyclostratigraphy from longer pelagic carbonate series in order to investigate for low frequency features in the modulations of the Milankovitch cycles that may prove useful in refining the astrochronological time scale.

Table 1

Astrochronologic ages of biomagnetostratigraphic events recorded in the Smirra section compared to the geochronologic ages of the GTS of Gradstein et al. (2012).

Magneto strat. chron	Planktonic foram. zone	Calc. nanno. zone	GTS 2012 age Ma	Smirra astrochron. age Ma
		CP12a–CP12b	47.8 ± 0.2	47.48 ± 0.05
C32r–C21n			47.3 ± 0.2	47.59 ± 0.05
Y–L boundary (within C21r)	E7a–E7b		47.8 ± 0.2	48.15 ± 0.05
			48.3 ± 0.2	48.21 ± 0.05
C22n–C21r			48.5 ± 0.2	48.80 ± 0.05

Note: The geochronologic age uncertainty of ± 0.2 Ma in the GTS 2012 (Gradstein et al., 2012 and references therein) is derived from 1s analytical error in extrapolated radioisotopic dates used to calibrate the Ypresian–Lutetian time scale; the uncertainty of ± 0.05 Ma in the astrochronologically calibrated ages of biomagnetostratigraphic events in the Smirra section is estimated from the stratigraphic uncertainty in the tuning (see Fig. 12) which is based on the correlation of the TLS time series band-pass filtered curve for the short eccentricity with eccentricity and location of a minimum in the long eccentricity from the La2010 nominal solution (Laskar et al., 2011).

Supplementary data to this article can be found online at <http://dx.doi.org/10.1016/j.palaeo.2015.08.027>.

Acknowledgments

The authors wish to thank Stefano Castelli (University of Padova) for assistance during TLS acquisitions at Smirra, Nereo Preto (University of Padova) and Giovanni Rusciadelli (University of Chieti) for help in the field work, and Mr. Marucchini for kindly allowing access to his Smirra quarry. Laura Peterson (Luther College) kindly revised the correctness of English. Suggestions by an anonymous reviewer greatly improved the quality of this paper. This work was partially supported by the Association “Le Montagne di San Francesco” of Coldigioco.

References

- Alvarez, W., Colacicchi, R., Montanari, A., 1985. Synsedimentary slides and bedding formation in: Apennines pelagic limestones. *J. Sediment. Res.* 55 (5), 720–734. <http://dx.doi.org/10.1306/212F87CE-2B24-11D7-8648000102C1865D>.
- Arthur, M.A., Fischer, A., 1977. Upper Cretaceous–Paleocene magnetic stratigraphy at Gubbio, Italy. I. Lithostratigraphy and sedimentology. *Geol. Soc. Am. Bull.* 88 (3), 367–371. [http://dx.doi.org/10.1130/0016-7606\(1977\)88<367:UCMAG>2.0.CO;2](http://dx.doi.org/10.1130/0016-7606(1977)88<367:UCMAG>2.0.CO;2).
- Aubry, M.P., 1999. Handbook of Cenozoic calcareous nannofossils. American Museum of Natural History 5. Micropress, New York, pp. 1–368.
- Batenburg, S.J., Sprovieri, M., Gale, A.S., Hilgen, F.J., Hüsing, S., Laskar, J., Liebrand, D., Lirer, F., Orue-Etxebarria, X., Pelosi, N., Smit, J., 2012. Cyclostratigraphy and astronomical tuning of the Late Maastrichtian at Zumaia (Basque contry, Northern Spain). *Earth Planet. Sci. Lett.* 359–360, 264–278. <http://dx.doi.org/10.1016/j.epsl.2012.09.054>.
- Bellian, J.A., Kerans, C., Jannette, D.C., 2005. Digital outcrop models: application of terrestrial scanning LIDAR technology in stratigraphic modeling. *J. Sed. Res.* 75 (2), 166–176.
- Besse, J., Courtillot, V., 2002. Apparent and true polar wander and the geometry of the geomagnetic field in the last 200 million years. *J. Geophys. Res.* 107. <http://dx.doi.org/10.1029/2000JB000050>.
- Bice, D., Montanari, A., Vučetić, V., Vučetić, M., 2012. The influence of regional and global climatic oscillations on Croatian climate. *Int. J. Climatol.* 32, 1537–1557. <http://dx.doi.org/10.1002/joc.2372>.
- Calcareous nannofossil biostratigraphy. In: Bown, P.R. (Ed.), British Micropalaeontological Society Publication Series. Chapman and Hall, pp. 1–315.
- Brown, R., Cleaveland, L., Bice, D.M., Koeberl, C., Montanari, A., 2009. Cyclostratigraphic analysis and astronomical tuning of the Eocene–Oligocene boundary GSSP at Massignano (Italy). In: Koeberl, C., Montanari, A. (Eds.), *The Late Eocene Earth. GSA Special Paper 452*, pp. 119–138.
- Burton, D., Dunlap, D.B., Wood, L.J., Flaig, P.P., 2011. Lidar intensity as a remote sensor of rock properties. *J. Sediment. Res.* 81, 339–347.
- Chan, L.S., Montanari, A., Alvarez, W., 1985. Magnetic stratigraphy of the Scaglia Rossa: implications for syndepositional tectonics of the Umbria–Marche basin, Italy. *Riv. Ital. Paleontol. Stratigr.* 91, 219–258.
- Cleaveland, L.C., Jensen, J., Goese, S., Bice, D.M., Montanari, A., 2002. Cyclostratigraphic analysis of pelagic carbonates at Monte dei Corvi (Ancona, Italy) and astronomical correlation of the Serravalian–Tortonian boundary. *Geology* 30 (10), 931–934. [http://dx.doi.org/10.1130/0091-7613\(2002\)030<0931:CAOPCA>2.0.CO;2](http://dx.doi.org/10.1130/0091-7613(2002)030<0931:CAOPCA>2.0.CO;2).
- Coccioni, R., Bancalà, G., 2012. New insights into the pattern, timing, and duration of the evolutionary origin of the foraminiferal genus *Hantkenina*. *Rev. Micropalaeontol.* 55, 71–81. <http://dx.doi.org/10.1016/j.rvmic.2012.03.002>.
- Coccioni, R., Marsili, A., Venturati, A., 2004. Chamber elongation in early Cretaceous planktonic foraminifera: a case study from the lower Hauterivian–lower Aptian Rio Argos succession (southern Spain). In: Coccioni, R., Galeotti, S., Lirer, F. (Eds.), *Proceedings of the First Italian Meeting on Environmental Micropaleontology 9*. Grzybowski Foundation Special Publication, pp. 37–47.
- Coccioni, R., Luciani, V., Marsili, A., 2006. Cretaceous oceanic anoxic events and radially elongated chambered planktonic foraminifera: paleoecological and paleoceanographic implications. *Palaeogeogr. Palaeoclimatol. Palaeoecol.* 235, 66–92.
- Coccioni, R., Premoli Silva, I., Marsili, A., Verga, D., 2007. First radiation of Cretaceous planktonic foraminifera with radially elongate chambers at Angles (Southeastern France) and biostratigraphic implications. *Rev. Micropalaeontol.* 50, 215–224.
- Coccioni, R., Marsili, A., Montanari, A., Bellanca, A., Neri, R., Bice, D.M., Brinkhuis, H., Church, N., Macalady, A., McDaniel, A., Deino, A., Lirer, F., Sprovieri, M., Maiorano, P., Monechi, S., Nini, C., Nocchi, M., Pross, J., Rochette, P., Sagnotti, L., Tateo, F., Yannick, T., Van Simaey, S., Williams, G.L., 2008. Integrated stratigraphy of the Oligocene pelagic sequence in the Umbria–Marche basin (northeastern Apennines, Italy): a potential Global Stratotype Section and Point (GSSP) for the Rupelian/Chattian boundary. *Geol. Soc. Am. Bull.* 120 (3–4), 487–511. <http://dx.doi.org/10.1130/B25988.1>.
- Coccioni, R., Sideri, M., Bancalà, G., Catanzariti, R., Frontalini, F., Jovane, L., Montanari, A., Savian, J., 2012a. Integrated stratigraphy (magneto-, bio- and chronostratigraphy) and geochronology of the Palaeogene pelagic succession of the Umbria–Marche Basin (central Italy). In: Jovane, L., Herrero-Bevera, E., Hinnov, L.A., Housen, B.A. (Eds.), *Magnetic Methods and Timing of Geological Processes*. Geological Society 373. Special Publications, London. <http://dx.doi.org/10.1144/SP373.4>.
- Coccioni, R., Bancalà, G., Catanzariti, R., Fornaciari, E., Frontalini, F., Giusberti, L., Jovane, L., Luciani, V., Savian, J., Sprovieri, M., 2012b. An integrated stratigraphic record of the

- Palaeocene–lower Eocene at Gubbio (Italy): new insights into the early Palaeogene hyperthermals and carbon isotope excursions. *Terra Nova* 24, 380–386. <http://dx.doi.org/10.1111/j.1365-3121.2012.01076.x>.
- Coccioni, R., Sideri, M., Banca, G., Catanzariti, R., Frontalini, F., Jovane, L., Montanari, A., Savian, J., 2013. Integrated stratigraphy (magneto-, bio- and chronostratigraphy) and geochronology of the Palaeogene pelagic succession of the Umbria–Marche Basin (central Italy). *Geological Society* 373. Special Publication, London, pp. 111–131. <http://dx.doi.org/10.1144/SP373.4>.
- Cogné, J.P., 2003. Paleomag: a Macintosh™ application for treating paleomagnetic data and making plate reconstructions. *Geochem. Geophys. Geosyst.* 4. <http://dx.doi.org/10.1029/2001GC000227>.
- D'Argenio, B., 1970. Evoluzione geotettonica comparata tra alcune piattaforme carbonatiche dei Mediterraneo Europeo ed Americano. *Atti Accad. Pontiana* 20, 3–34.
- Dercourt, J., Ricou, L.E., Vrielynck, B., 1993. *Atlas Tethys Palaeoenvironmental Maps*: Paris. Gauthier Villars (307 p).
- Franceschi, M., Teza, G., Preto, N., Pesci, A., Galgaro, A., Girardi, S., 2009. Discrimination between marls and limestones using intensity data from terrestrial laser scanner. *ISPRS J. Photogramm. Remote Sens.* 64, 522–528.
- Franceschi, M., Preto, N., Hinnov, L.A., Huang, C., Rusciadelli, G., 2011. Terrestrial laser scanner imaging reveals astronomical forcing in the early Cretaceous of the Tethys realm. *Earth Planet. Sci. Lett.* 305, 359–370. <http://dx.doi.org/10.1016/j.epsl.2011.03.017>.
- Galeotti, S., Krishnan, S., Pagani, M., Lanci, L., Gaudio, A., Zachos, J.C., Monechi, S., Morelli, G., Lourens, L.J., 2010. Orbital chronology of Early Eocene hyperthermals from the Contessa Road section, central Italy. *Earth Planet. Sci. Lett.* 290, 192–200. <http://dx.doi.org/10.1016/j.epsl.2009.12.021>.
- Gardin, S., Galbrun, B., Thibault, N., Coccioni, R., Premoli Silva, I., 2012. Bio-magnetostratigraphy for the upper Campanian–Maastrichtian from the Gubbio area, Italy: new results from the Contessa Highway and Bottaccione sections. *Newsl. Stratigr.* 45, 75–103.
- Giusberti, L., Coccioni, R., Sprovieri, M., Tateo, F., 2009. Perturbation at the sea floor during the Paleocene–Eocene Thermal Maximum: evidence from benthic foraminifera at Contessa Road, Italy. *Mar. Micropaleontol.* 70, 102–119. <http://dx.doi.org/10.1016/j.micropaleo.2008.11.003>.
- Gradstein, F., Ogg, J., Schmitz, M., Ogg, G., 2012. *The Geologic Time Scale*. Elsevier, Amsterdam.
- Herbert, T.D., Fischer, A.G., 1986. Milankovitch climatic origin of black shale rhythms in central Italy. *Nature* 321, 739–743.
- Hinnov, L.A., 2000. New perspectives on orbitally forced stratigraphy. *Annu. Rev. Earth Planet. Sci. Lett.* 28, 419–475.
- Hinnov, L.A., 2013. Cyclostratigraphy and its revolutionizing applications in the earth and planetary sciences. *Geol. Soc. Am. Bull.* 125 (11–12), 1703–1734.
- Hinnov, L.A., Ogg, J., 2007. Cyclostratigraphy and the astronomical time scale. *Stratigraphy* 4, 239–251.
- Hüsing, S.K., Cascella, A., Hilgen, F.J., Krijgsman, W., Kuiper, K.F., Turco, E., Wilson, D., 2010. Astrochronology of the Mediterranean Langhian between 15.29 and 14.17 Ma. *Earth Planet. Sci. Lett.* 290 (3–4), 254–259. <http://dx.doi.org/10.1016/j.epsl.2009.12.002>.
- Hyland, E., Murphy, B., Varela, P., Marks, K., Colwell, L., Tori, F., Monechi, S., Cleaveland, L., Brinkhuis, H., van Mourik, C.A., Coccioni, R., Bice, D., Montanari, A., 2009. Integrated stratigraphic and astrochronologic calibration of the Eocene–Oligocene transition in the Monte Cagnero section (northeastern Apennines, Italy): a potential parastatotype for the Messinian global stratotype section and point (GSSP). *Geol. Soc. Am. Spec. Pap.* 452, 303–322. [http://dx.doi.org/10.1130/2009.2452\(19\)](http://dx.doi.org/10.1130/2009.2452(19)).
- Johnsson, M.J., Reynolds, R.C., 1986. Clay mineralogy of shale–limestone rhythmites in the Scaglia Rossa (Turonian–Eocene), Italian Apennines. *J. Sediment. Petrol.* 54 (4), 501–509. <http://dx.doi.org/10.1306/212F896D-2B24-11D7-8648000102C1865D>.
- Jovane, L., Florindo, F., Coccioni, R., Dinarès-Turell, J., Marsili, A., Monechi, S., Roberts, A.P., Sprovieri, M., 2007. The middle Eocene climatic optimum event in the Contessa Highway section, Umbrian Apennines, Italy. *Geol. Soc. Am. Bull.* 119, 413–427.
- Jovane, L., Sprovieri, M., Coccioni, R., Florindo, F., Marsili, F., Laskar, J., 2010. Astronomical calibration of the middle Eocene Contessa Highway section (Gubbio, Italy). *Earth Planet. Sci. Lett.* 298, 77–88. <http://dx.doi.org/10.1016/j.epsl.2010.07.027>.
- Kapellos, C., Schaub, H., 1973. Zur Korrelation von Biozonierung mit Grossforaminiferen und Nannoplankton im Paläogen der Pyrenäen. *Ecologe Geol. Helv.* 66, 687–737.
- Kirshvink, J.L., 1980. The least-squares line and plane and the analysis of paleomagnetic data. *Geophys. J. R. Astron. Soc.* 62, 699–718.
- Larrasoña, J.C., Gonzalvo, C., Molina, E., Monechi, S., Ortiz, S., Tori, F., Tosquella, J., 2008. Integrated magnetostratigraphy of the Early/Middle Eocene transition at Agost (Spain): Implications for defining the Ypresian/Lutetian boundary stratotype. *Lethaia* 41, 395–415.
- Laskar, J., Robutel, P., Joutel, F., Gastineau, M., Correia, A.C.M., Levrard, B., 2004. A long term numerical solution for the insolation quantities of the Earth. *Astron. Astrophys.* 428, 261–285.
- Laskar, J., Fienga, A., Gastineau, M., Manche, H., 2011. La2010: a new orbital solution for the long-term motion of the Earth. *Astron. Astrophys.* 532 (A89). <http://dx.doi.org/10.1051/0004-6361/201116836>.
- Lirer, F., 2000. A new technique for retrieving calcareous microfossils from lithified lime Deposits. *Micropaleontology* 46, 365–369.
- Lourens, L.J., Sluijs, A., Kroon, D., Zachos, J.C., Thomas, E., Röhl, U., Bowles, J., Raffi, I., 2005. Astronomical pacing of late Palaeocene to early Eocene global warming events. *Nature* 435, 1083–1087. <http://dx.doi.org/10.1038/nature03814>.
- Lowrie, W., Alvarez, W., Napoleone, G., Perch-Nielsen, P., Silva, I.P., Tourmarkine, M., 1982. Paleogene magnetic stratigraphy in Umbrian pelagic carbonate rocks: the Contessa sections, Gubbio (Italy). *Geol. Soc. Am. Bull.* 93 (5), 414–432. [http://dx.doi.org/10.1130/0016-7606\(1982\)93<414:PMSIUP>2.0.CO;2](http://dx.doi.org/10.1130/0016-7606(1982)93<414:PMSIUP>2.0.CO;2).
- Luciani, V., Giusberti, L., 2014. Reassessment of the early–middle Eocene planktic foraminiferal biomagnetostratigraphy: New evidence from the Tethyan Possagno section (NE Italy) and western North Atlantic Ocean ODP Sites 1051. *J. Foraminif. Res.* 44, 187–201.
- Mader, D., Cleaveland, L., Koeberl, C., Bice, D., Montanari, A., 2004. High-resolution geochemical proxies of a short Langhian pelagic sequence at the Cònero Riviera, Ancona (Italy): some palaeoenvironmental and cyclostratigraphic considerations. *Paleogeogr. Paleoclimatol. Paleocool.* 211, 325–344.
- Martini, E., 1971. Standard Tertiary and Quaternary calcareous nannoplankton zonation. In: Farinacci, A. (Ed.), *Proceedings of the Second Planktonic Conference, Rome 1970*. 2. Tecnoscienza, Rome, pp. 739–785.
- McFadden, P.L., McElhinny, M.W., 1990. Classification of the reversal test in paleomagnetism. *Geophys. J. Int.* 103, 725–729.
- Molina, E., Alegret, L., Apellaniz, E., Bernaola, G., Caballero, F., Dinarès-Turell, J., Hardenbol, J., Heilmann-Clausen, C., Larrasoña, J.C., Luterbacher, H., Monechi, S., Ortiz, S., Orue-Etxebarria, X., Payros, A., Pujalte, V., Rodríguez-Tovar, F.J., Tori, F., Tosquella, J., Uchman, A., 2011. The Global Standard Stratotype Section and Point (GSSP) for the base of the Lutetian Stage at the Gorronatxe section, Spain. *Episodes* 34, 86–108.
- Montanari, A., Chan, L.S., Alvarez, W., 1989. Synsedimentary tectonics in the Late Cretaceous–Early Tertiary pelagic basin of the Northern Apennines. In: Crevello, P., Wilson, J.L., Sarg, R., Reed, F. (Eds.), 44. *SEPM Special Publication*, pp. 379–399.
- Montanari, A., Bice, D.M., Coccioni, R., Deino, A., DePaolo, D.J., Emmanuel, L., Renard, M., Monechi, G., Zevenboom, D., 1997. Integrated stratigraphy of the Chattian to mid Burdigalian pelagic sequence of the Contessa Valley (Gubbio, Italy). In: Montanari, A., Odin, G.S., Coccioni, R. (Eds.), *Miocene Stratigraphy: An Integrated Approach Developments in Paleontology and Stratigraphy* 15. Elsevier Science B.V., pp. 249–278.
- Muller, R.A., MacDonald, G.J., 2000. Ice ages and astronomical causes. *Data, Spectral Analysis and Mechanisms*. Springer, London, p. 318.
- Muttoni, G., Argani, A., Kent, D.V., Abrahamsen, N., Cibin, U., 1998. Paleomagnetic evidence for Neogene tectonic rotations in the northern Apennines, Italy. *Earth Planet. Sci. Lett.* 154, 25–40.
- Okada, H., Bukry, D., 1980. Supplementary modification and introduction of code numbers to the low-latitude coccolith biostratigraphic zonation (Bukry, 1973; 1975). *Mar. Micropaleontol.* 5C, 321–325.
- Olsen, P.E., Kent, D.V., 1996. Milankovitch climate forcing in the tropics of Pangaea during the Late Triassic. *Paleogeogr. Paleoclimatol. Paleocool.* 122, 1–26.
- Payros, A., Orue-Etxebarria, X., Bernaola, G., Apellaniz, E., Dinarès-Turell, J., Tosquella, J., Caballero, F., 2009. Characterization and astronomically calibrated age of the first occurrence of *Turborotalia frontosa* in the Gorronatxe section, a prospective Lutetian GSSP: implications for the Eocene time scale. *Lethaia* 42, 255–264.
- Payros, A., Dinarès-Turell, J., Bernaola, G., Orue-Etxebarria, X., Apellaniz, E., Tosquella, J., 2010. On the age of the Early/Middle Eocene boundary and other related events: cyclostratigraphic refinements from the Pyrenean Otsakar section and the Lutetian GSSP. *Geol. Mag.* 148, 442–460.
- Pearson, P.N., Olsson, R.K., Huber, B.T., Hemleben, C., Berggren, W.A., 2006. *Atlas of Eocene Planktonic Foraminifera*. Special Publication 41. Cushman Foundation for Foraminiferal Research, pp. 1–514.
- Penasa, L., Franceschi, M., Preto, N., Teza, G., Polito, V., 2014. Integration of intensity textures and local geometry descriptors from Terrestrial Laser Scanning to map chert in outcrops. *ISPRS J. Photogramm. Remote Sens.* 93, 88–97. <http://dx.doi.org/10.1016/j.isprsjprs.2014.04.003>.
- Perch-Nielsen, K., 1985. Mesozoic calcareous nannofossils. In: Bolli, H.H., Saunders, J.B., Perch-Nielsen, K. (Eds.), *Plankton Stratigraphy*. Cambridge University Press, pp. 329–426.
- Pesci, A., Teza, G., 2008. Effects of surface irregularities on intensity data from laser scanning: an experimental approach. *Ann. Geophys.* 5 (5/6), 829–848.
- Schwarzacher, W., 2005. The stratification and cyclicity of the Dachstein Limestone in Lofer, Leogang and Steinernes Meer (Northern Calcareous Alps, Austria). *Sediment. Geol.* 118, 93–106.
- Tori, F., Monechi, S., 2013. Lutetian calcareous nannofossil events in the Agost section (Spain): implications toward a revision of the Middle Eocene biomagnetostratigraphy. *Lethaia* 46, 293–307.
- Varol, O., 1989. Eocene calcareous nannofossils from Sile (northwest Turkey). *Rev. Esp. Micropaleontol.* 21, 273–320.
- Wade, B.S., Pearson, P.N., Berggren, W.A., Pälike, H., 2011. Review and revision of Cenozoic tropical planktic foraminiferal biostratigraphy and calibration to the geomagnetic polarity and astronomical time scale. *Earth Sci. Rev.* 104, 111–142. <http://dx.doi.org/10.1016/j.earscirev.2010.09.003>.
- Westerhold, T., Röhl, U., Laskar, J., Raffi, I., Bowles, J., Lourens, L.J., Zachos, J.C., 2007. On the duration of magnetochrons C24r and C25n and the timing of early Eocene global warming events: implications from the Ocean Drilling Program Leg 208Walvis Ridge depth transect. *Paleoceanography* 22, PA2201. <http://dx.doi.org/10.1029/2006PA001322>.